Published in final edited form as:
Acta Biomater. 2015 October 1; 25: 284–290. doi:10.1016/j.actbio.2015.06.037.

The role of ROS generation from magnetic nanoparticles in an alternating magnetic field on cytotoxicity

Robert J. Wydra[1], **Piotr G. Rychahou**[2], **B. Mark Evers**[2,3], **Kimberly W. Anderson**[1], **Thomas D. Dziubla**[1], and **J. Zach Hilt**[1,*]

[1] Department of Chemical and Materials Engineering, University of Kentucky, KY 40506, USA

[2]Department of Surgery, College of Medicine, University of Kentucky, KY 40506, USA

[3]Markey Cancer Center, University of Kentucky, Lexington, KY 40506, USA

Abstract

Monosaccharide coated iron oxide nanoparticles were developed to selectively target colon cancer cell lines for magnetically mediated energy delivery therapy. The nanoparticles were prepared using a coupling reaction to attach the glucose functional group to the iron oxide core, and functionality was confirmed with physicochemical characterization techniques. The targeted nanoparticles were internalized into CT26 cells at a greater extent than non-targeted nanoparticles, and the nanoparticles were shown to be localized within lysosomes. Cells with internalized nanoparticles were exposed to an AMF to determine the potential to delivery therapy. Cellular ROS generation and apoptotic cell death was enhanced with field exposure. The nanoparticle coatings inhibit the Fenton-like surface generation of ROS suggesting a thermal or mechanical effect is more likely the source of the intracellular effect.

Keywords

iron oxide; glyconanoparticles; magnetically mediated energy delivery; reactive oxygen species

1. Introduction

Magnetic nanoparticles are being studied for a wide range of biomedical applications such as diagnostic imaging, drug delivery, and thermal therapy of cancer [1-4]. In the case of thermal therapy, the particles absorb the energy from the magnetic field and convert it into heat through the Brownian and Neel relaxation [5]. In most cases, the nanoparticles rely on passive targeting to systemically circulate and accumulate in tumors via the phenomenon known as the enhanced permeability and retention effect [6]. To increase specific interactions with cells, nanoparticles can be functionalized with appropriate targeting ligands

---

[*] Contact Author: J. Zach Hilt, Associate Professor of Chemical Engineering, Department of Chemical and Materials Engineering, University of Kentucky, 177 F. Paul Anderson Tower, Lexington, KY 40506-0046, Tel.: +1-859-257-9844, Fax: +1-859-323-1929, hilt@engr.uky.edu.

such as peptides, antibodies, and carbohydrates [7-9]. It has recently been demonstrated that targeted nanoparticles are not only capable of reaching the primary tumor but micrometastatic sites as well [10]. Coupled with the ground breaking work by Creixell et al. demonstrating that internalized targeted nanoparticles can induce cellular death when exposed to an alternating magnetic field without a measurable temperature rise, there is great interest to develop targeted nanoparticles for the treatment of metastatic cancer [11]. This intracellular effect, where the internalized nanoparticles deliver therapeutic gains without perceived temperature rise, has been coined as ‘magnetically mediated energy delivery’ (MagMED) represents a promising field of therapeutics but the exact mechanism of cytotoxicity still needs to be explored [12].

Intracellular hyperthermia was previously considered improbable due to heat transport calculations by Rabin that demonstrated theoretically the heat generated from a single nanoparticle or cluster of nanoparticles would be negligible to the cell or surrounding tumor [13]. However, it has been observed that the surface temperature of the nanoparticles is able to significantly exceed the solution temperature suggesting that a localized heating effect may attribute to the toxicity of the therapy [14]. In addition to a heating effect, chemical effects or mechanical damage from the physical rotation and vibration of the nanoparticles may induce toxicity. One potential chemical effect would be the result of surface mediated production of reactive oxygen species (ROS) from the iron oxide nanoparticles [15]. Free radical generation results in cellular oxidative stress which is believed to be one of the key underlying mechanisms of cytotoxicity [16, 17]. When temperatures are raised to the hyperthermia range, ROS levels are amplified resulting in long-term cellular death [18]. This observation can be attributed to increased kinetic activity of the Fenton-like reaction with temperature or the decreased ability of cancer cells to scavenge ROS at the elevated temperature [18-20]. Recently, we have demonstrated that the generation of ROS is enhanced in presence of an alternating magnetic field [21]. At nanoparticle concentrations where there was no observable temperature rise, we observed a significant increase in ROS generation compared to the Arrhenius prediction.

Carbohydrate coated nanoparticles, or glyconanoparticles, are an attractive functionality in order to study molecular and cellular targeting by combining the physicochemical properties of the core nanoparticle with receptor interaction, stabilization, and relatively inexpensive compared to other targeting ligands (i.e. antibodies) advantages from carbohydrates [22-26]. Functionalizing nanoparticles with monosaccharides can provide similar passivation to poly(ethylene glycol) (PEG) while at the same time providing a targeting strategy for cells overexpressing glucose transporters [27-29]. Demonstrating therapeutic potential, gold nanoparticles functionalized with glucose were internalized at a greater rate by ovarian cancer cells and used as a sensitizer to enhance radiation therapy [30]. Specifically, we were interested in designing a nanoparticle system to target colon cancer liver metastasis. To date, fluorine-18-deoxyglucose has been successful in the accurate detection of colon cancer liver metastases with positron emission tomography suggesting glucose may be an interesting ligand to study [31].

In this paper, monosaccharide coated nanoparticles were developed and assessed for their ability to be selectively internalized by colon cancer cell lines. Glucose coated nanoparticles were synthesized using a two-step process. Iron oxide core nanoparticles, selected for their ability to remotely heat in an AMF, were prepared utilizing a facile one-pot co-precipitation technique where a citric acid stabilizer was added during the core synthesis. Next, glucose functionality was attached to the surface through an amine-carboxyl coupling reaction involving D-glucosamine and the citric acid stabilizer. Due to the hypothesized increased interactions with cancer cells, the glucose coated particles are referred to as targeted compared to the non-targeted counterparts of uncoated and citric acid coated nanoparticles studied in comparison. Once internalized, the cells containing nanoparticles were exposed to an alternating magnetic field and cellular ROS was measured. After exposure, we observed a significant increase in cellular ROS and an associated increased level of apoptotic cells.

2. Materials and Methods

2.1 Materials

Iron (III) chloride hexahydrate ($FeCl_3 \cdot 6H_2O$), iron (II) chloride tetrahydrate ($FeCl_2 \cdot 4H_2O$), D-(+)-glucosamine, and fluoresceinamine isomer I were obtained from Sigma Aldrich (St Louis, MO). Ammonium hydroxide (NH_4OH) was obtained from EMD Chemicals (Gibbstown, NJ). Citric acid monohydrate (CA) was obtained from Fisher Scientific and N-hydroxysuccinimide (NHS) and 1-ethyl-3-(3-dimethylaminopropyl) carbodiimide (EDC) were obtained from Thermo Scientific (Waltham, MA). All materials were used as received.

2.2 Synthesis of iron oxide nanoparticles

A one-pot co-precipitation method was used to prepare the core citric acid coated iron oxide nanoparticles as reported previously [32]. Briefly, aqueous solutions of $FeCl_3 \cdot 6H_2O$ and $FeCl_2.4H_2O$ were combined in a 2:1 molar ratio in a sealed three-neck flask under vigorous stirring and an inert N_2 environment. Once 85 °C was reached, 5 mL of NH_4OH was injected into the vessel followed by 4 ml of 2 M citric acid. The reaction was carried out for 1 hour. The particles were transferred to a dialysis tube for 24 hours of dialysis to remove unreacted chemicals.

2.3 Glucose functionalization

Monosaccharide functional groups were attached to the nanoparticle surface through an amine-carboxyl coupling reaction utilizing NHS/EDC. A molar ratio of 10:1 molar EDC to carboxyl groups was used where the amount of citric acid per nanoparticle was estimated from TGA data. The NHS to EDC ratio was 5:2 molar and glucosamine was used in 10 fold by mass excess to the amount of nanoparticles. In a typical reaction, a stock 10 mg/ml suspension of citric acid coated nanoparticles was mixed with EDC/NHS in aqueous solution to facilitate activation of the carboxyl groups for 30 minutes. Glucosamine solution was prepared in PBS and added to the work up for a final working concentration of 5 mg/ml nanoparticles and allowed to react for 6 hours. Following the reaction, the nanoparticles were washed with dialysis.

2.4 Particle characterization

2.4.1 Fourier Transform infrared (FTIR) spectra—Attenuated total reflectance FTIR (ATR-FTIR) was used to determine surface functionalization with a Varian Inc. 7000e spectrometer. Dried samples were placed on the diamond ATR crystal and the spectrum was obtained between 700 and 4000 cm^{-1} for 32 scans.

2.4.2 Thermal gravimetric analysis (TGA)—TGA was used to quantify the mass percent of the iron oxide core particle. Measurements were performed using a TA Instruments SDT Q600 TGA/DSC instrument (New Castle, DE). Approximately 10 mg of dried sample was loaded and a heat rate of 5 °C/min under constant nitrogen flow was used. At 120 °C, the sample was held isothermal for 10 minutes to vaporize residual solvent and potential water vapor from the atmosphere. The sample continued to heat at 5 °C/min until 450 °C. The presented values are normalized to the mass at 120 °C.

2.4.3 Dynamic Light Scattering (DLS) and zeta potential—DLS and zeta potential measurements were obtained using a Malvern Zetasizer, Nano ZS90 instrument (Westborough, MA). Nanoparticles from stock suspensions were diluted in DI water for DLS and 10 mM NaCl to a concentration of 200 μg/mL and dispersed via probe sonication.

2.6 Uptake and Localization

CT26 colorectal cancer cells were cultured in Dulbecco's Modified Eagle's Medium supplemented with 10 % v/v calf bovine serum, 10 μg/mL Fungizone (Invitrogen, Carlsbad, CA), and 2 μg/mL Penicillin-Streptomycin-Glutamine (ATCC) in an incubator at 37°C and 5% CO_2. The cells were seeded in a 35 mm culture dishes at 15000 cells/cm^2 and were allowed to become confluent. Dehydrated nanoparticles were suspended in DMSO at 5 mg/ml stock concentration. DMSO was used as a co-solvent to improve the stability of the uncoated nanoparticles when diluted in cell culture media. The nanoparticles were diluted to 200 μg/ml in cell media prior to exposure. The cells were exposed to nanoparticles for 0.5, 1, and 2 hours. After, the cells were washed 2x with warm DPBS, trypsinized, counted, and dehydrated prior to the Prussian Blue colorimetric assay. 100 μl HCl was used to digest the dry cell pellet and 10 μl of the digested pellet was transferred to a microcentrifuge tube where the reducing agent, hydroxylamine, was added for at least 8 hours. Finally, the iron ions were stained with a 5% potassium ferricyanide solution for 1 hour. Absorbance at 700 nm was measured with a GENios Pro fluorescence spectrophotometer (Tecan, Switzerland). Iron concentration standard curves were prepared using ferrous and ferric chloride salts.

To visualize the nanoparticle internalization a co-localization technique was utilized. First, the nanoparticles were fluorescently tagged with fluoresceinamine, isomer I through a competitive carboxyl-amine coupling reaction. The reaction work-up and purification was the same as the glucose functionalization step described above with a fluoresceinamine isomer I to glucosamine ratio of 0.02:1. The fluorescently tagged nanoparticles were diluted to 50 μg/ml and incubated with CT26 cells overnight. The cells were washed 2x with DPBS and stained with DAPI and Lysotracker Red. Post staining, the cells were imaged utilizing a fluorescent microscope and analyzed for internalization (Nikon Elements 4.2).

2.7 Cellular Response to Alternating Magnetic Field

Similar to above, CT26 cells were seeded in a 35 mm culture dishes at 15000 cells/cm^2 and were allowed to become confluent. The cells were doped with iron oxide nanoparticles from

5 mg/ml DMSO stocks and incubated for an additional 1 hour. The media was removed, washed 2x with warm DPBS, and cells were detached using trypsin. Cells were split into samples with and without field exposure and doped with 50 mM 6-carboxy-2',7'-dichlorodihydrofluorescein diacetate (carboxy-DCFDA) (Invitrogen). Cells were incubated at 37 °C for 30 minutes to facilitate stain internalization, exposed to the field for 30 minutes (Taylor Winfield magnetic induction source; approximately 60 kA/m in strength at 292 kHz frequency), and returned to the incubator for 30 minute post incubation. Cells were analyzed using an Accuri C6 flow cytometer (BD Biosciences, San Jose, CA). A ratio of the mean fluorescence between samples exposed to the AMF and the samples that remained in the incubator was used to determine the enhanced ROS generation attributed to the nanoparticles in the AMF.

To determine the effects of the treatment, a Caspase 3/7 Apoptosis assay (Invitrogen) was utilized. Following the intracellular procedure described above, the cells were stained with the reagent per the manufactures protocol immediately following the AMF exposure and allowed to incubate for 30 minutes. After the incubation period the cells were analyzed with flow cytometry. A ratio of the mean fluorescence between samples exposed to the AMF and the samples that remained in the incubator was used to assess the effects of the field exposure.

2.8 Surface ROS Generation

To determine the amount of ROS generated from the surface the nanoparticles a methylene blue degradation assay was used. The degradation experiments were performed in 2 ml microcentrifuge tubes where one ml samples were prepared by diluting stock concentrations of methylene blue to 5 μg/ml and iron oxide nanoparticles to 75 μg/ml. The samples were placed in the water bath for 10 min to equilibrate to the expected steady state temperature as a result of field exposure. The degradation was initiated by spiking the samples with 30% H_2O_2 to a working concentration of 245 mM. The samples were exposed to a field of approximately 51.0 kA/m in strength at 292 kHz frequency while temperature was measured with a Luxtron FOT Lab Kit. After given time intervals the samples were centrifuged for 30 s using a Phenix Quickspin Centrifuge, magnetically decanted, and measured using UV-visible spectroscopy (maximum absorbance at 665 nm) with a Varian Cary. To account for nanoparticle scattering from the nanoparticles that remain in suspension, samples containing only nanoparticles were measured and subtracted out from the sample absorbance.

2.9 Statistical Analysis

Statistical analysis of the ROS generation and apoptosis assay were performed using ANOVA and a post hoc two sample Student's t-test comparing fluorescent ratios to the control. To indicate significant differences defined by the following ranges: $p < 0.05$, $p < 0.01$ and $p < 0.001$, a single, double, or triple asterisk was included in the figures.

3. Results and Discussion

3.1 Characterization of nanoparticles

Following the reaction, the nanoparticles were characterized to confirm the success of the functionalization. FTIR was utilized as an initial screen to verify the presence of predicted functional groups. In **figure 1**, there is a change in signature between the citric acid and the glucose coated nanoparticles with the key peaks of interest being a shoulder at 1088 cm^{-1} attributed to the C-N vibration and a pronounced peak at 1040 cm^{-1} indicating the location of C-O stretch peak attributed to the glucosamine. It should be noted that the loss of the primary amine peak from glucosamine further confirms a covalent bond instead of electrostatic interactions between the carboxyl and amine groups. With citric acid stabilized iron oxide, Wu et al. previously observed a shift in carbonyl stretch from the typical 1700 cm^{-1} to an intense band at 1614 cm^{-1} to indicate the citric acid radical binding to the iron oxide surface [33]. Similarly, our nanoparticles display a shift to 1560 cm^{-1} and this intense band will overlap with the carbonyl from the amide. Thus, the distinct differences in FTIR spectra come from C-N stretching and C-O stretching from the D-glucosamine.

In **figure 2**, TGA indicated similar mass loss for both citrate and glucose coated particles, approximately 10 and 12% respectively, however a change in the profile was observed indicating different compounds. The citrate coating displayed its greatest mass loss between 150 and 200 °C which is similar to the values reported by Frimpong et al. [32]. Glucose coated particles saw its greatest mass loss shift to between 200 and 300 °C.

The nanoparticle systems were further characterized with DLS and Zeta Potential to determine the hydrodynamic size of the particles and surface charge (**table 1**). Citrate coated nanoparticles were 75 nm in diameter with a PDI of 0.207 and glucose functionalized particles were 70 nm with a PDI of 0.193. The addition of the monosaccharide functional group resulted in no increase in hydrodynamic size. This result also indicated that there was no aggregation induced during the additional synthesis and washing steps. Previous work with TEM has determined the core iron oxide crystal size to be on the order of 10 nm and the uncoated nanoparticles have a hydrodynamic size of around 100 nm attributed to a lack of aqueous stabilizer. The zeta potential displays a distinct shift from −34.7 to −20.3 mV. During the functionalization step, carboxyl groups from the stabilizing agent are being partially replaced by the monosaccharide molecules resulting in a diminished surface charge.

3.2 Uptake and Localization

A Prussian blue colorimetric assay was used to quantify cellular uptake of uncoated, citric acid coated, and glucose coated iron oxide nanoparticles into CT26 cells. In **figure 3**, the glucose coated nanoparticles display a greater extent of internalization compared to the non-targeted nanoparticles. Over the three time points measured, glucose coated nanoparticles display a 2-3 fold increase over the citric acid coated nanoparticles. Internalization of the glucose coated nanoparticles increased with time and slightly more than doubles between 0.5 and 2 hours. The internalization of the uncoated nanoparticles remains relatively constant between 5-8 pg iron per cell. Citric acid coated nanoparticle internalization doubles between 0.5 and 1 hour but then remains constant.

To visualize the location of the nanoparticles in CT26 cells, the glucose coated iron oxide nanoparticles were functionalized with a green fluorescent tag. Co-localization studies were performed with the addition of DAPI blue and Lyso-tracker red stains to visualize the location of the nucleus and lysosomes respectively. Representative images can be found below in **figure 4**. In the control figure, there is a diminished presence of naturally occurring lysosomes. In the case of nanoparticle exposure, there are areas of yellow-orange overlap from the green nanoparticles and red lysosomes suggesting the nanoparticles are being internalized in lysosomes. Previously, it was determined that glucose coated iron oxide nanoparticles were internalized by cells via a caveolae dependent pathway culminating in lysosomes [34]. While working with similarly designed glucose functionalized nanoparticles, Shan et al. studied the effects of using a GLUT-1 inhibitor on the rate of internalization [28]. They determined that the internalization was retarded to rates similar to control nanoparticle system. However, glucose transporters are more attuned to transporting small molecules across the cell membrane, not nanoparticles on the order of 70 nm. We picture that the glucose functionalized nanoparticles are sticking to the cell surface via glucose transporters, internalized via caveolae, and eventually compartmentalized into lysosomes.

3.3 Alternating Magnetic Field Response

After determining the selectivity of the glucose coated nanoparticles, cells with internalized nanoparticles were exposed to the AMF to demonstrate the potential of the system to deliver MagMED therapy. To study the changes in cellular ROS levels, a DCFDA assay was used. In the presence of ROS, the acetate groups are cleaved converting the molecule from non-fluorescent to fluorescent. The cells were exposed to the AMF for 30 minutes while the temperature was measured with a Luxtron FOT Lab Kit. At the power setting used (approximately 60 kA/m in strength at 292 kHz frequency), the radiant heat from the copper coil heated cellular media to 37-38.5 °C, and there was no difference in heating profile between the control group and the nanoparticle systems. The presence of nanoparticles altered the absolute measured fluorescent value, so a ratio of samples exposed to the AMF and the samples that remained in the incubator was used. Using a ratio of measured fluorescence would account for any stress induced by the nanoparticles previously observed in concentration dependent toxicity studies [16]. **Figure 5** displays the field enhancement ratio of the various systems tested with CT26 cells. There is negligible enhancement in the control group, and any minor increase was attributed to deviation away from ideal culture conditions. Significant enhancement was observed with nanoparticle exposure. Glucose coated nanoparticles displayed an additional enhancement compared to the other non-targeted nanoparticle systems. The increase in ROS enhancement is thought to be associated with the amount of nanoparticles internalized by the cells.

Increased intracellular ROS generation from engineered nanomaterials typically leads to a cytotoxic event. A Caspase 3/7 Apoptosis assay was utilized to determine the effects of the increased ROS enhancement and to demonstrate the potential as a therapeutic. Through the activation of caspase 3/7 in apoptotic cells, the reagent is activated and becomes fluorescent when bound with cellular DNA. Similar to above, **figure 6** displays the ratio of fluorescent values between exposed to the AMF, and the samples that remained in the incubator. Only the glucose coated nanoparticles displayed a significant increase in caspase 3/7 activity compared to the control and the non-targeted nanoparticle systems. The increase in ROS generation during AMF exposure is capable of the triggering the apoptotic pathway leading the cellular death.

To determine the source of the ROS generation, we examined the surface generation through a methylene blue dye degradation assay. The surfaces of iron oxide nanoparticles are capable of catalytically generating ROS through the Fenton and Haber-Weiss reactions. In a Fenton-like system, iron ions react with hydrogen peroxide to generate highly reactive hydroxyl and superoxide radicals which in turn attack bonds on methylene blue fracturing the molecule into colorless intermediates. By measuring methylene blue colorimetrically, the amount of degradation can be determined. **Figure 7** below displays the amount of methylene blue degraded by the various nanoparticle systems when exposed to the AMF for 5 or 15 minutes. The concentration of nanoparticles selected was 75 μg/ml where there is minimum, 1.5 °C, temperature rise of the solution attributed to nanoparticle heating. Previously at this concentration we observed a statistical enhancement in ROS generation with uncoated nanoparticles compared with the Arrhenius prediction [21]. The uncoated nanoparticles display significant degradation on the order of 40-60%. However, the coated systems display negligible degradation indicating our coating inhibits the Fenton-like reaction.

Toxicity associated with iron oxide nanoparticles is typically attributed to Fenton-like catalytic generation of free radicals with endogenous hydrogen peroxide [35, 36]. Based on previous results, our initial hypothesis was cellular ROS generation would be enhanced through the local heating of the nanoparticles driving the Fenton-like chemistry. Since our coated systems do not display this behavior suggests that another mechanism is at play beyond a chemical effect. In the presence of the alternating magnetic field, the nanoparticles would be physically rotating and realigning themselves with the field. If bound to the cell membrane or internalized within lysosomes these physical motions would induce stress within the cell. The ROS generation in response to these physical stresses would correspond with the amount of nanoparticles internalized. In the case of EGFR targeted iron oxide nanoparticles, Domenech et al. observed an increase in lysosomal permeability correlating with increased ROS generation and decreased viability as a result of their intracellular treatment [37]. They attributed this observation to heat dissipation or mechanical disruption of the lysosomes. Similarly, iron oxide nanoparticles were coated with lysosomal protein marker antibodies to specifically accumulate along the lysosome membrane [38]. In this case, the alternating magnetic field applied was at 20 Hz where only physical rotations by the nanoparticles would be actuated. The resulting cellular apoptosis occurred due to the lysosomal disruption from the rotational forces.

Accounting for the location of the nanoparticles in lysosomes, the shift in pH (μ4.5) would result in some dissolution of iron oxide to iron ions. These free ions have the potential to leave the lysosome to the cytosol, mitochondria, or endoplasmic reticulum where they would encounter conditions more favorable to Fenton-like chemistry in terms of available hydrogen peroxide [35, 39-42]. The toxicity of iron oxide nanoparticles has been directly tied to intracellular release of iron ions which would react with mitochondrial hydrogen peroxide [43]. Considering the theoretical heating calculations, there remains doubt whether the nanoscale heating isolated in lysosomes would be able to effect the kinetics in neighboring organelles [13, 44]. Experimental evidence demonstrating nanoscale heating involves changes in a fluorescent polymeric shell or nanoparticles in the direct vicinity of a liposomal carrier increasing the permeability of the bilayer [14, 45, 46]. Lysosomal membrane permeabilization from free radicals has been demonstrated by elevating the intralysosomal iron content through iron loaded silica particles [47, 48]. The source of the intralysosomal hydrogen peroxide is a direct result of membrane bound NADPH oxidase stimulation by the silica particles [49]. However, uncoated iron oxide nanoparticles do not similarly stimulate NADPH oxidase with endocytosis [50]. Thus in our case, even if the coating is displaced, the only potential source of lysosomal hydrogen peroxide available would have to escape catalase degradation and freely diffuse into the compartment.

With our specific nanoparticle systems, we can likely eliminate a chemical effect and point to either a thermal or mechanical effect disrupting the lysosomal membrane as the source of enhanced ROS generation and associated apoptosis. Future work is still warranted to determine the exact mechanism of cytotoxicity for our system. Despite the above results, the chemical effect should not be ignored in future MagMED research. Different coatings could display different degrees of reactivity or a biodegradable coating could be developed resulting in an uncoated nanoparticle when internalized. The local energy delivered could be used to enhance the efficacy of chemotherapeutics exploiting the altered redox state of cancer cells. Beyond mechanistic studies, *in vivo* studies are warranted demonstrating the potential of this therapy. By not relying on bulk heating, one of the proposed advantages is that with an appropriate targeting strategy the injection dosage required can be lowered such that there is minimal healthy tissue toxicity.

4. Conclusions

This study reports the use glucose coated iron oxide nanoparticles for the selective internalization and assessed for their potential to deliver MagMED therapy to a colorectal cancer cell line. The targeted nanoparticles displayed increased internalization compared to non-targeted nanoparticles, and co-localization suggests the nanoparticles are internalized into lysosomes. With exposure of an alternating magnetic field, the glucose coated nanoparticles displayed a significant increase in cellular ROS and apoptotic cell death with no measurable increase in media temperature. To determine if the mechanism of toxicity was attributed to a chemical effect, we investigated the surface generation of ROS through Fenton-like chemistry. The coated systems displayed negligible ROS generation compared to uncoated nanoparticles. These observations suggest the cellular ROS measured is attributed to a thermal or mechanical effect of the internalized nanoparticles.

Acknowledgments

RW acknowledges the financial support from a NCI-CNTC pre-doctoral traineeship and the project described was supported by Grant Number R25CA153954 from the National Cancer Institute. The content is solely the responsibility of the authors and does not necessarily represent the official views of the National Cancer Institute or the National Institutes of Health.

References

1. Frimpong RA, Hilt JZ. Magnetic nanoparticles in biomedicine: synthesis, functionalization and applications. Nanomedicine. 2010; 5:1401–14. [PubMed: 21128722]
2. Berry CC. Progress in functionalization of magnetic nanoparticles for applications in biomedicine. Journal of Physics D-Applied Physics. 2009; 42:9.
3. Ito A, Shinkai M, Honda H, Kobayashi T. Medical application of functionalized magnetic nanoparticles. Journal of Bioscience and Bioengineering. 2005; 100:1–11. [PubMed: 16233845]
4. Sun C, Lee JSH, Zhang MQ. Magnetic nanoparticles in MR imaging and drug delivery. Advanced Drug Delivery Reviews. 2008; 60:1252–65. [PubMed: 18558452]
5. Hilger I, Dietmar E, Linss W, Streck S, Kaiser WA. Developments for the minimally invasive treatment of tumours by targeted magnetic heating. Journal of Physics-Condensed Matter. 2006; 18:S2951–S8.
6. Iyer AK, Khaled G, Fang J, Maeda H. Exploiting the enhanced permeability and retention effect for tumor targeting. Drug Discovery Today. 2006; 11:812–8. [PubMed: 16935749]
7. De la Fuente JM, Penades S. Glyconanoparticles: Types, synthesis and applications in glycoscience, biomedicine and material science. Biochimica Et Biophysica Acta-General Subjects. 2006; 1760:636–51.
8. Sunderland CJ, Steiert M, Talmadge JE, Derfus AM, Barry SE. Targeted nanoparticles for detecting and treating cancer. Drug Development Research. 2006; 67:70–93.
9. Kruse AM, Meenach SA, Anderson KW, Hilt JZ. Synthesis and characterization of CREKA-conjugated iron oxide nanoparticles for hyperthermia applications. Acta Biomaterialia. 2014; 10:2622–9. [PubMed: 24486913]
10. Kievit FM, Stephen ZR, Veiseh O, Arami H, Wang T, Lai VP, et al. Targeting of Primary Breast Cancers and Metastases in a Transgenic Mouse Model Using Rationally Designed Multifunctional SPIONs. ACS nano. 2012; 6:2591–601. [PubMed: 22324543]
11. Creixell M, Bohorquez AC, Torres-Lugo M, Rinaldi C. EGFR-Targeted Magnetic Nanoparticle Heaters Kill Cancer Cells without a Perceptible Temperature Rise. ACS nano. 2011; 5:7124–9. [PubMed: 21838221]
12. Kozissnik B, Bohorquez AC, Dobson J, Rinaldi C. Magnetic fluid hyperthermia: Advances, challenges, and opportunity. International Journal of Hyperthermia. 2013; 29:706–14. [PubMed: 24106927]
13. Rabin Y. Is intracellular hyperthermia superior to extracellular hyperthermia in the thermal sense? International Journal of Hyperthermia. 2002; 18:194–202. [PubMed: 12028637]
14. Polo-Corrales L, Rinaldi C. Monitoring iron oxide nanoparticle surface temperature in an alternating magnetic field using thermoresponsive fluorescent polymers. Journal of Applied Physics. 2012; 111:3.
15. Voinov MA, Pagan JOS, Morrison E, Smirnova TI, Smirnov AI. Surface-Mediated Production of Hydroxyl Radicals as a Mechanism of Iron Oxide Nanoparticle Biotoxicity. Journal of the American Chemical Society. 2011; 133:35–41. [PubMed: 21141957]
16. Cochran DB, Wattamwar PP, Wydra R, Hilt JZ, Anderson KW, Eitel RE, et al. Suppressing iron oxide nanoparticle toxicity by vascular targeted antioxidant polymer nanoparticles. Biomaterials. 2013; 34:9615–22. [PubMed: 24016851]
17. Naqvi S, Samim M, Abdin MZ, Ahmed FJ, Maitra AN, Prashant CK, et al. Concentration-dependent toxicity of iron oxide nanoparticles mediated by increased oxidative stress. International Journal of Nanomedicine. 2010; 5:983–9. [PubMed: 21187917]
18. Sadhukha T, Niu L, Wiedmann TS, Panyam J. Effective Elimination of Cancer Stem Cells by Magnetic Hyperthermia. Molecular Pharmaceutics. 2013; 10:1432–41. [PubMed: 23432410]
19. Ghosh P, Kumar C, Samanta AN, Ray S. Comparison of a new immobilized Fe3+ catalyst with homogeneous Fe3+-H2O2 system for degradation of 2,4-dinitrophenol. Journal of Chemical Technology and Biotechnology. 2012; 87:914–23.

20. Seton-Rogers S. CANCER STEM CELLS Survival skills. Nature Reviews Cancer. 2009; 9:147.
21. Wydra RJ, Oliver CE, Anderson KW, Dziubla TD, Hilt JZ. Accelerated generation of free radicals by iron oxide nanoparticles in the presence of an alternating magnetic field. RSC Adv. 2015; 5:18888–93. [PubMed: 25798231]
22. Marradi M, Chiodo F, Garcia I, Penades S. Glyconanoparticles as multifunctional and multimodal carbohydrate systems. Chemical Society Reviews. 2013; 42:4728–45. [PubMed: 23288339]
23. El-Boubbou K, Huang XF. Glyco-Nanomaterials: Translating Insights from the "Sugar-Code" to Biomedical Applications. Current Medicinal Chemistry. 2011; 18:2060–78. [PubMed: 21517769]
24. Li X, Bao MM, Weng YY, Yang K, Zhang WD, Chen GJ. Glycopolymer-coated iron oxide nanoparticles: shape-controlled synthesis and cellular uptake. Journal of Materials Chemistry B. 2014; 2:5569–75.
25. Li X, Zhou H, Yang L, Du G, Pai-Panandiker AS, Huang X, et al. Enhancement of cell recognition in vitro by dual-ligand cancer targeting gold nanoparticles. Biomaterials. 2011; 32:2540–5. [PubMed: 21232787]
26. Schmidtke C, Kreuziger AM, Alpers D, Jacobsen A, Leshch Y, Eggers R, et al. Glycoconjugated Amphiphilic Polymers via Click-Chemistry for the Encapsulation of Quantum Dots. Langmuir. 2013; 29:12593–600. [PubMed: 24028496]
27. Moros M, Pelaz B, Lopez-Larrubia P, Garcia-Martin ML, Grazu V, de la Fuente JM. Engineering biofunctional magnetic nanoparticles for biotechnological applications. Nanoscale. 2010; 2:1746–55. [PubMed: 20676420]
28. Shan XH, Hu H, Xiong F, Gu N, Geng XD, Zhu W, et al. Targeting Glut1-overexpressing MDA-MB-231 cells with 2-deoxy-d-g1ucose modified SPIOs. European Journal of Radiology. 2012; 81:95–9. [PubMed: 21440393]
29. Xiong F, Zhu Z-y, Xiong C, Hua X-q, Shan X-h, Zhang Y, et al. Preparation, Characterization of 2-Deoxy-D-Glucose Functionalized Dimercaptosuccinic Acid-Coated Maghemite Nanoparticles for Targeting Tumor Cells. Pharmaceutical Research. 2012; 29:1087–97. [PubMed: 22173782]
30. Geng F, Song K, Xing JZ, Yuan CZ, Yan S, Yang QF, et al. Thio-glucose bound gold nanoparticles enhance radio-cytotoxic targeting of ovarian cancer. Nanotechnology. 2011:22.
31. Zhuang H, Sinha P, Pourdehnad M, Duarte PS, Yamamoto AJ, Alavi A. The role of positron emission tomography with fluorine-18-deoxyglucose in identifying colorectal cancer metastases to liver. Nuclear Medicine Communications. 2000; 21:793–8. [PubMed: 11065150]
32. Frimpong RA, Dou J, Pechan M, Hilt JZ. Enhancing remote controlled heating characteristics in hydrophilic magnetite nanoparticles via facile co-precipitation. Journal of Magnetism and Magnetic Materials. 2010; 322:326–31.
33. Wu X, Tan Y, Mao H, Zhang M. Toxic effects of iron oxide nanoparticles on human umbilical vein endothelial cells. International Journal of Nanomedicine. 2010; 5:385–99. [PubMed: 20957160]
34. Moros M, Hernaez B, Garet E, Dias JT, Saez B, Grazu V, et al. Monosaccharides versus PEG Functionalized NPs: Influence in the Cellular Uptake. ACS nano. 2012; 6:1565–77. [PubMed: 22214244]
35. Wang B, Yin JJ, Zhou XY, Kurash I, Chai ZF, Zhao YL, et al. Physicochemical Origin for Free Radical Generation of Iron Oxide Nanoparticles in Biomicroenvironment: Catalytic Activities Mediated by Surface Chemical States. Journal of Physical Chemistry C. 2013; 117:383–92.
36. Singh N, Manshian B, Jenkins GJS, Griffiths SM, Williams PM, Maffeis TGG, et al. NanoGenotoxicology: The DNA damaging potential of engineered nanomaterials. Biomaterials. 2009; 30:3891–914. [PubMed: 19427031]
37. Domenech M, Marrero-Berrios I, Torres-Lugo M, Rinaldi C. Lysosomal Membrane Permeabilization by Targeted Magnetic Nanoparticles in Alternating Magnetic Fields. ACS nano. 2013; 7:5091–101. [PubMed: 23705969]
38. Zhang EM, Kircher MF, Koch M, Eliasson L, Goldberg SN, Renstrom E. Dynamic Magnetic Fields Remote-Control Apoptosis via Nanoparticle Rotation. ACS nano. 2014; 8:3192–201. [PubMed: 24597847]

39. Klein S, Sommer A, Distel LVR, Neuhuber W, Kryschi C. Superparamagnetic iron oxide nanoparticles as radiosensitizer via enhanced reactive oxygen species formation. Biochemical and Biophysical Research Communications. 2012; 425:393–7. [PubMed: 22842461]
40. Valko M, Rhodes CJ, Moncol J, Izakovic M, Mazur M. Free radicals, metals and antioxidants in oxidative stress-induced cancer. Chemico-Biological Interactions. 2006; 160:1–40. [PubMed: 16430879]
41. Joshi-Barr S, Lux CD, Mahmoud E, Almutairi A. Exploiting Oxidative Microenvironments in the Body as Triggers for Drug Delivery Systems. Antioxidants & Redox Signaling. 2014; 21:730–54. [PubMed: 24328819]
42. Schieber M, Chandel NS. ROS Function in Redox Signaling and Oxidative Stress. Current Biology. 2014; 24:R453–R62. [PubMed: 24845678]
43. Malvindi MA, De Matteis V, Galeone A, Brunetti V, Anyfantis GC, Athanassiou A, et al. Toxicity Assessment of Silica Coated Iron Oxide Nanoparticles and Biocompatibility Improvement by Surface Engineering. Plos One. 2014:9.
44. Keblinski P, Cahill DG, Bodapati A, Sullivan CR, Taton TA. Limits of localized heating by electromagnetically excited nanoparticles. Journal of Applied Physics. 2006:100.
45. Huang H, Delikanli S, Zeng H, Ferkey DM, Pralle A. Remote control of ion channels and neurons through magnetic-field heating of nanoparticles. Nature Nanotechnology. 2010; 5:602–6.
46. Amstad E, Kohlbrecher J, Muller E, Schweizer T, Textor M, Reimhult E. Triggered Release from Liposomes through Magnetic Actuation of Iron Oxide Nanoparticle Containing Membranes. Nano Letters. 2011; 11:1664–70. [PubMed: 21351741]
47. Persson HL. Iron-dependent lysosomal destabilization initiates silica-induced apoptosis in murine macrophages. Toxicology Letters. 2005; 159:124–33. [PubMed: 15949905]
48. Johansson AC, Appelqvist H, Nilsson C, Kagedal K, Roberg K, Ollinger K. Regulation of apoptosis-associated lysosomal membrane permeabilization. Apoptosis. 2010; 15:527–40. [PubMed: 20077016]
49. Persson HL. Radiation-induced lysosomal iron reactivity: Implications for radioprotective therapy. Iubmb Life. 2006; 58:395–401. [PubMed: 16801214]
50. Yu M, Huang SH, Yu KJ, Clyne AM. Dextran and Polymer Polyethylene Glycol (PEG) Coating Reduce Both 5 and 30 nm Iron Oxide Nanoparticle Cytotoxicity in 2D and 3D Cell Culture. International Journal of Molecular Sciences. 2012; 13:5554–70. [PubMed: 22754315]

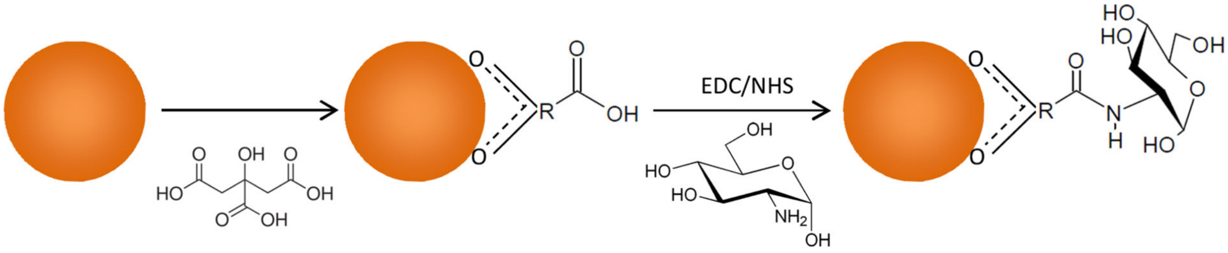

Scheme 1.

Reaction schematic of monosaccharide coating of iron oxide nanoparticles displaying the attachment of the citric acid stabilizer and subsequent addition of D-glucosamine via amine-carboxyl coupling reaction

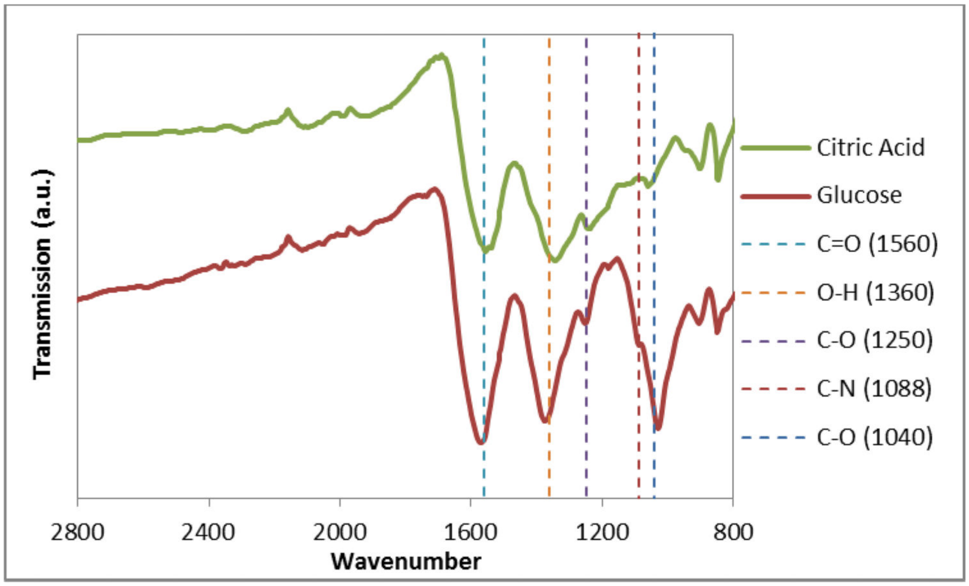

Figure 1.

FTIR spectra of citric acid coated iron oxide and glucose coated samples. The vertical line at 1088 cm^{-1} indicates the location of a C-N vibration and at 1040 cm^{-1} indicated the location of C-O stretch peak attributed to the D-glucosamine. The vertical lines 1560 cm^{-1}, 1360 cm^{-1}, and 1250 cm^{-1} indicate the location of the C=O stretch, O-H bend, and C-O stretch bonds, respectively, typically attributed to citric acid coated particles.

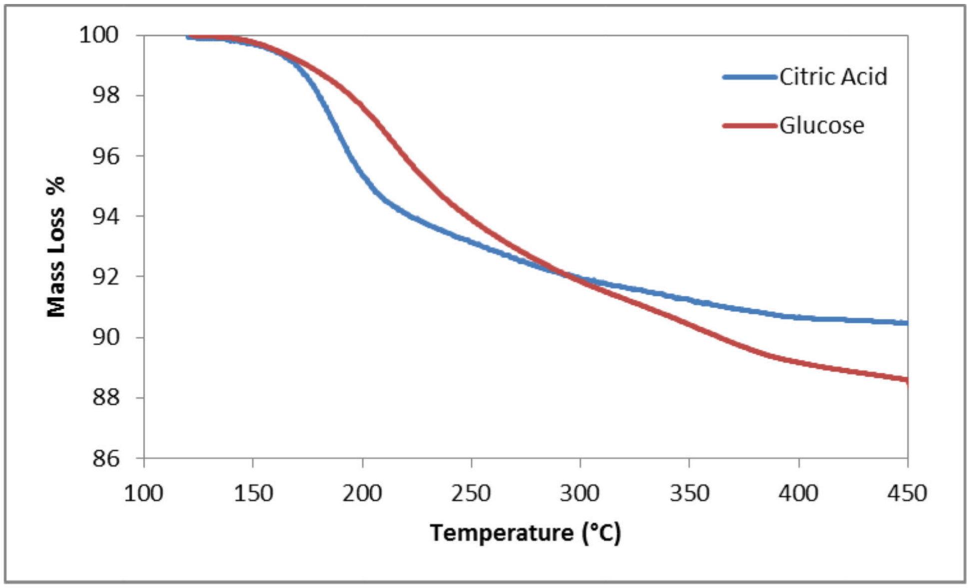

Figure 2.

Mass loss profile of citric acid and glucose coated iron oxide.

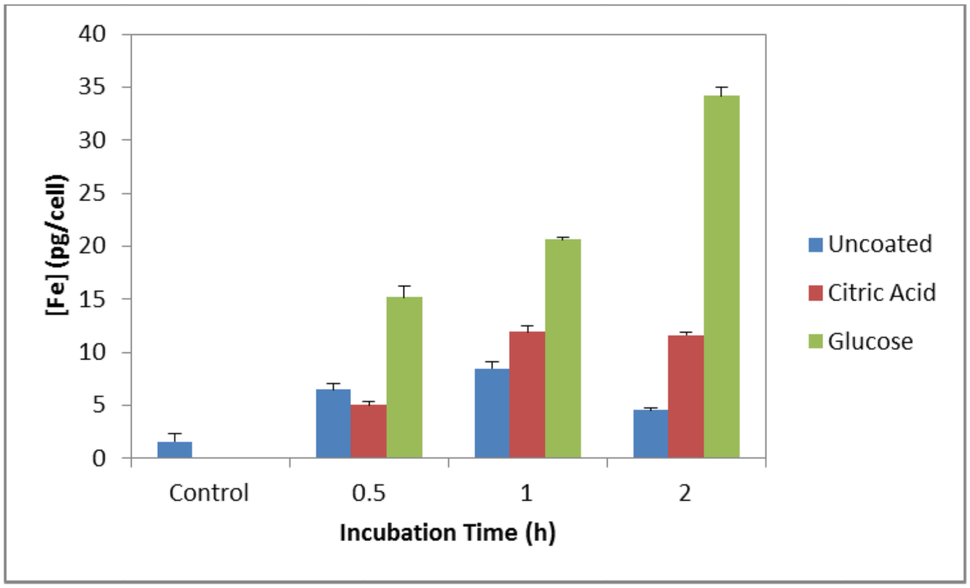

Figure 3.

Iron content in CT26 cells when exposed to 200 μg/ml of nanoparticles over 0.5, 1, and 2 hours of incubation. Control group consists of cells never exposed to nanoparticles but underwent similar culturing conditions.

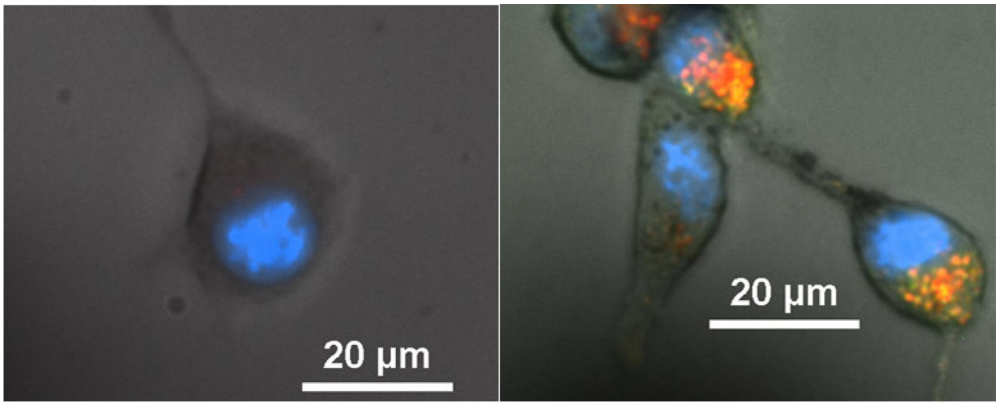

Figure 4.

Representative localization images of control (a) and 50 μg/ml fluorescently tagged glucose coated nanoparticles (b) incubated with CT26 cells.

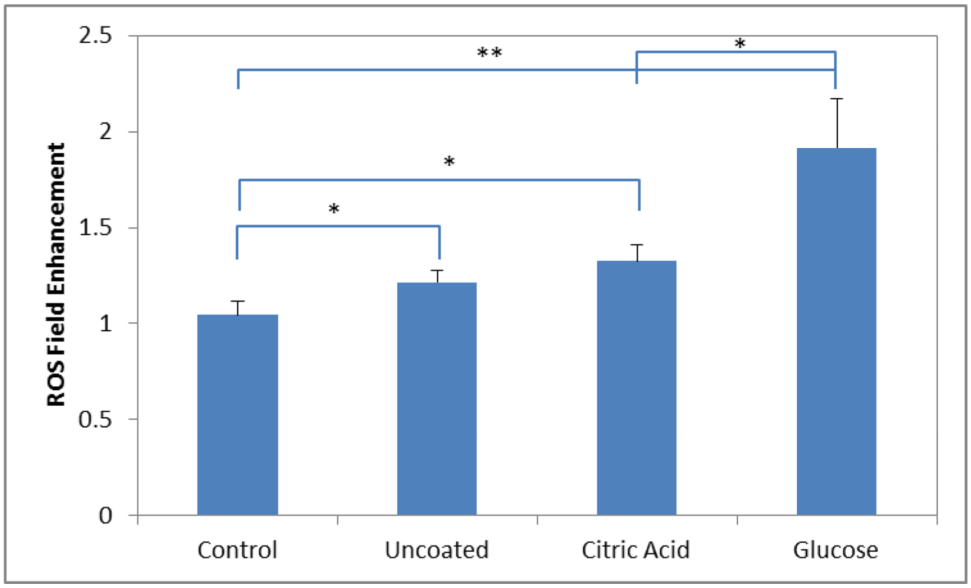

Figure 5.

Measured ROS enhancement with field exposure determined by dividing the relative fluorescent means from the samples with field exposure by no field exposure. Significant differences between groups are indicated as *$p < 0.05$, **$p < 0.01$.

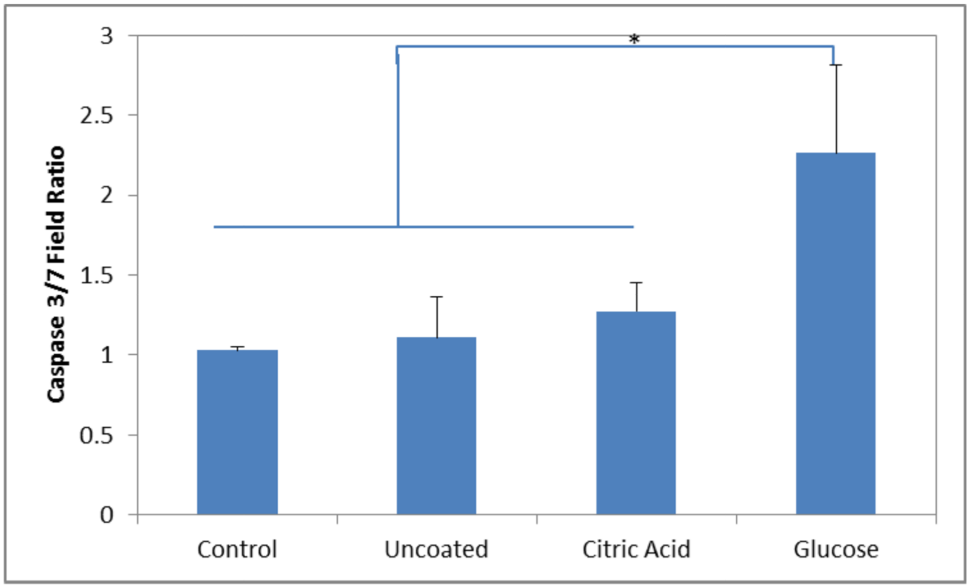

Figure 6.

Ratio of Caspase 3/7 fluorescence of cells with and without field exposure when exposed to various nanoparticle systems. Significant differences between groups are indicated as $*p < 0.05$.

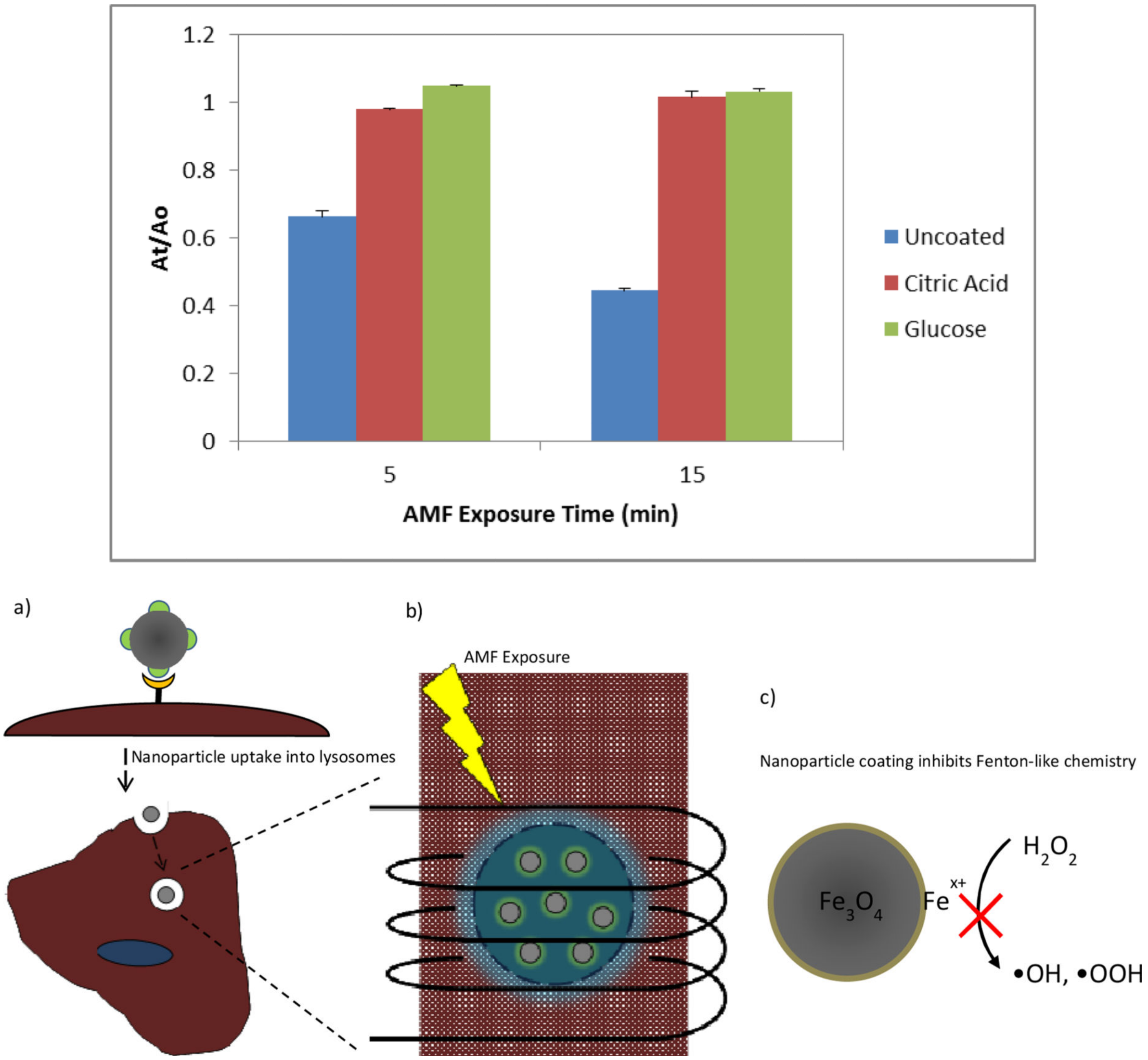

Figure 7.

Fenton-like generation of ROS by nanoparticle systems measured by methylene blue dye degradation. 75 μg/ml nanoparticles were exposed to the AMF for 5 and 15 minutes in the presence of 0.75% H_2O_2.

(a) Targeted magnetic nanoparticles bind to cell surface and are internalized into lysosomes. (b) AMF activation induces lysosomal permeability triggering cellular death. (c) Nanoparticle coating inhibits Fenton-like chemistry indicating a thermal or mechanical effect causes the lysosomal disruption.

Table 1

Results from DLS and Zeta potential measurements of coated nanoparticles.

	Zavg (nm)	PDI	Zeta (mV)
Citric Acid	75.36	0.207	−34.7
Glucose	70.06	0.193	−20.3